J Intell Robot Syst (2010) 57:505–529
DOI 10.1007/s10846-009-9368-0

Design Methodology of a Hybrid Propulsion Driven Electric Powered Miniature Tailsitter Unmanned Aerial Vehicle

Mirac Aksugur · Gokhan Inalhan

Received: 1 February 2009 / Accepted: 1 August 2009 / Published online: 17 September 2009

Abstract Contrary to the manned tailsitter aircraft concepts, which have been shelved and forgotten after mid 1960's, the unmanned versions of these concepts have become popular. Since, tailsitter type UAVs combine both vertical takeoff and landing (VTOL) operation and relatively high speed cruise flight capabilities which provide manifest advantages over the other VTOL aircraft concepts, including helicopters and organic air vehicles (OAVs). However, there is no mini class tailsitter UAV with efficient high speed cruise flight capability. This paper presents the design methodology and optimization of ITU Tailsitter UAV concept with hybrid propulsion system approach to fill that gap. The initial design and analysis show the advantageous performance over other mini-class VTOL UAVs.

Keywords VTOL · Tailsitter · UAV · Electric propulsion

1 Introduction

Tailsitter UAVs combine vertical takeoff and landing (VTOL) operation and relatively high speed cruise capabilities in a single airframe and such a concept provides manifest advantages over the other VTOL aircraft concepts including helicopters and organic air vehicles (OAVs). As a result of the increasing demand for efficient and silent UAV concepts which require no regular "runway" for urban-civilian applications, the design of ITU-BYU tailsitter concept is tailored towards city and urban operations with possible autonomous recharging capability to allow 24 hour

M. Aksugur (✉) · G. Inalhan
Controls and Avionics Lab, Faculty of Aeronautics and Astronautics,
Istanbul Technical University, Istanbul, Turkey
e-mail: aksugur@itu.edu.tr

G. Inalhan
e-mail: inalhan@itu.edu.tr

on demand reconnaissance and surveillance for various usage areas from traffic/law-enforcement to border patrol.

The design and development of manned tailsitter concepts had begun in the beginning of 1950s and many experimental aircraft were built and tested during the period between 1950 and 1960s. The pilots of such manned aircraft were in charge of the aircraft's attitude control by only looking at the displays and sensing the behaviors of the aircraft in an upside position with unfamiliar control inputs compared to the helicopter pilots. Moreover, such manned aircraft had control problems especially during landing and hover-to-cruise transition phase, because of having no stability augmentation system to help decrease test pilots' extremely high workload. Therefore, none of the experimental tailsitter concepts have demonstrated an apparent advantage over helicopters or fixed wing aircraft. As a result of several accidents mainly due to the high workload of the test pilots, the development of manned tailsitter projects were suspended after mid 1960s. However, with the help of the advances in both hardware and software based technologies [4, 6, 14], the distinct tailsitter concept was finally successfully developed to take its place among the other VTOL UAVs. Likewise, there are many already mature or under development VTOL concepts. At the present time, OAVs are the most popular ones which can be classified under tailsitter concepts. Allied Aerospace's iStar series Organic Air vehicles (OAV) and Honeywell's electric powered mini class OAV are the foremost examples with a wide range of application around the world. On the other hand, although the OAVs show efficient static-low speed flight due to the shroud and duct around the propeller blades, such ducted fan UAV concepts still have some aerodynamic problems, especially in efficient forward flight regime and hoverto-cruise transition phase. In addition, OAVs with internal combustion engines also suffer from high levels of noise during operationwhich making these types of tailsitter UAVs unsuitable for "silent intelligence" in urban operational areas. Other examples of mini to mid size tailsitter concepts are T-Wing and Heli- wing. T-Wing was developed at University of Sydney at 2000s [21], and Heliwing was developed by Boeing. However, both of these similar concepts are not suitable size wise for urban applications because of their noisy internal combustion engines. Besides, there are also several micro class tailsitter UAV concepts such as Brigham Young University's tailsitter UAV [13] and University of Arizona's coaxial propeller driven UAV [18]. Nevertheless, such micro size UAVs are not suitable for carrying a "useful" payload and for service in severe weather conditions. Two of the discussed tailsitter concepts are seen in Fig. 1.

Since 2001, related to the recent progress in Lithium based batteries, aircraft designers have started to consider electric powered aircraft concepts [16]. Moreover, advances in brushless DC electric motors have accelerated the development period of such kind of aircraft. Selection of an electric propulsion system for ITU Tailsitter was a major pre-design choice and brings with it the advantages of low noise levels, easier maintenance and the unique capability to autonomously recharge the units from base landing stations. However, for an electric powered vehicle within the mini-UAV class, this unique capability calls for a trade-off between speed limited high power propeller configuration and the power limited high speed electric ducted fan (EDF) system. In this study for mini class UAVs, design optimization and an intuitive thrust-power-airspeed trade-off approach, which leads to a hybrid "propeller-ducted fan propulsion system" design that can achieve maximum horizontal flight time and

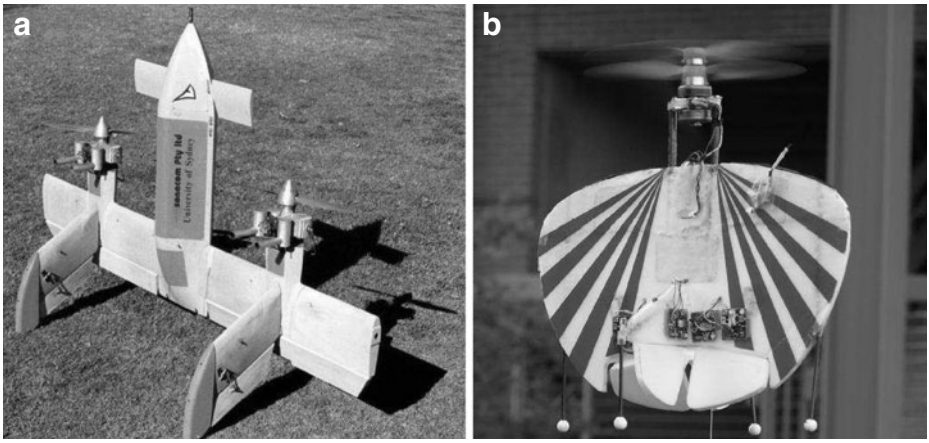

Fig. 1 **a** T-wing concept demonstrator from University of Sydney [1], **b** micro tailsitter UAV prototype from University of Arizona [18]

maximum range for the ongoing ITU Tailsitter Project, is presented. As a result, the hybrid propulsion system, consisting of both propulsion systems, was decided to be used in order to design an "all flight regime" efficient aircraft which meets the desired requirements.

Due to the aim of designing an efficient tailsitter UAV, propulsion system has the highest priority among the design requirements. Since electric powered propulsion system has advantages over internal combustion engines in terms of maintenance and noise level; it has been chosen as one of the requirements. Propeller driven system supplies high thrust to power ratio for VTOL operations. However, the thrust is rapidly decreased as the incoming airspeed is increased. Hence, the performance is decreased at high speed and the system becomes insufficient for cruise flight. On the other hand, Electric EDF systems are capable of producing the same thrust with a higher thrust to power gradient than the propeller systems. Although the power consumption is increased, EDF system's thrust is necessary only for long range cruise operations.

In ITU Tailsitter, a folding propeller system, located on the nose of the aircraft, is used for hovering, vertical take-off, vertical landing and low-speed transition mode, whereas an EDF system, which is placed between the stabilizers, is used for level and high speed flight modes where the propeller folds onto the fuselage in order to reduce drag when it is turned off. In addition, to calculate the approximate empty weight, instead of the classic method of empty weight fraction, an "aircraft-based" weight modeling and optimization study have been conducted so as to see the most efficient design possible. Initial system performance analysis with candidate propulsion units has shown that up to 40m/s cruise speed and maximum 120 min of flight endurance can be achieved while carrying 1 kg of payload in 10kg of flying system with 3 min of vertical take-off and landing operation duration—a distinct performance in comparison to the same class rotary-wing and OAV alternatives. In the following sections, a trade off analysis is presented where the hybrid-dual propulsion approach with a qualitative analysis of the selected propulsion systems,

is described. This is followed by the design overview and the design and design optimization approach. Finally, the control methodology and the results are denoted.

2 Trade-off Analysis

For the most-energy-efficient flight, although a hybrid dual propulsion technique seems to be the ideal approach for this class of UAVs, a two-fold alternative trade-off can be considered in detail.

First trade-off in consideration is the usage of a big EDF-only propulsion system instead of the hybrid system. The reason for such a choice is that we can utilize propeller propulsion system's weight for extra batteries for enhanced mission duration. However, even if the EDF-only configuration seems advantageous over the hybrid propulsion system initially, there are two main problems. The first one is the efficiency problem such that during hover conditions, the states of the aircraft are controlled by the aerodynamic force generator surfaces that are influenced by propulsion system's air-wash. Therefore, placing such force generator vanes with servo actuators behind the EDF unit adds not only extra weight to the empty weight of the aircraft but also reduces the efficiency of the propulsion system both in hover and in cruise condition because of the additional drag. As a result, using the hybrid propulsion system increases the flight efficiency and aircraft's controllability during VTOL and transition operations. Because, similar to the 3D-aerobatic model airplanes; hover, vertical ascent and vertical descent maneuvers are controlled via propeller's induced velocity on relatively large and high deflection angle control surfaces at the tail of the aircraft. Moreover, after transition from vertical ascent to cruise flight, as the EDF system is activated, the folding propellers fold onto the fuselage and the drag component of the propeller propulsion system is minimized.

Second is a trade off between larger ducted fan systems called Organic Aerial Vehicles (OAVs) and the tailsitter aircraft with hybrid propulsion system. Ducted fan UAVs (OAVs) which have shrouded propellers are advantageous over the propeller only systems. Nevertheless, there are three main disadvantages of OAVs. First of all, for the forward flight case, OAVs require excessive thrust because of wing loading and drag force that is created by both the large duct and aircraft's weight component. Second, the variable pitch system adds more weight which results in reduced payload capacity. Third, as a result of increasing parasite drag of the duct; ducted system loses its efficiency as the airspeed increases [20].

Besides the two trade-off explanations, figure of merit (FOM) chart consisting of VTOL only systems, can be seen in Fig. 2. Note that, the point rating is limited between -1 and 1, where -1 is a negative and 1 is a positive effect on the total points. "VPP" stands for "Variable Pitch Propeller" in the FOM chart. the concept with hybrid propulsion system is the foremost one which is followed by the single propeller driven and twin propeller driven (T-Wing, Heliwing) tailsitter concepts, as evident from the comparison. Note that, OAV concept has the lowest rank among the other concepts being examined. Therefore, before starting the design process, the FOM chart has shown the advantages of the concept equipped with hybrid/dual propulsion system.

Figure of Merit (FOM)	Agility	Payload capacity	Endurance	High speed performance	Cruise efficiency	Development time	Ease of build	Complexity	TOTAL
One propeller driven	1	1	0	-1	-1	1	1	1	3
Coaxial propeller driven	1	0	-1	-1	0	-1	-1	-1	-4
OAV	-1	0	-1	-1	-1	0	-1	0	-5
Twin propeller driven	1	0	0	-1	0	1	1	0	2
Ducted propeller-at-tail	0	0	-1	-1	0	-1	-1	-1	-5
One propeller driven w/ VPP	1	-1	-1	1	1	-1	-1	-1	-2
Coaxial propeller driven w/ VPP	1	-1	-1	1	1	-1	-1	-1	-2
OAV w/ VPP	-1	-1	-1	0	0	-1	-1	-1	-6
Twin propeller driven w/ VPP	1	-1	-1	1	1	-1	-1	-1	-2
Ducted propeller-at-tail w/ VPP	0	-1	-1	0	1	-1	-1	-1	-4
Hybrid propulsion driven	1	1	1	1	1	1	1	1	8

Fig. 2 Figure of merit of different types of VTOL tailsitter aircraft

3 Hybrid-dual Propulsion Approach

In addition to aerodynamic design, selection of the right propulsion system/component is has utmost importance for the determination of the performance of an aircraft. Comparing the propulsion systems of both "heavy lifter" helicopter and "fast and agile" jet fighter, it can be comprehended that relatively high diameter and low weight loading propeller blades are efficient for hovering whereas relatively small diameter blades having high induced velocity are used as an effective way to reach high speeds. After an inspection of the COTS (Commercial Off The Shelf) equipment available on the market, the hybrid propulsion concept is specified with a folding propeller having a 28.5 in. diameter and an EDF system with a 4 in. diameter placed in a single airframe. In this section, both propulsion systems are described with a qualitative comparison. This is followed by the scaled specific thrust concept, which shows the advantages of combined/hybrid propulsion system quantitatively.

3.1 Qualitative Comparison of the Propulsion Systems

The information given in this section is for clarifying the facts about both type of propulsion systems. General characteristics of both propeller and EDF systems are presented based on the wind tunnel test and analytical calculations.

3.1.1 Propeller Propulsion System

To select the appropriate propeller for an aircraft, all the performance data of the candidate propellers should be carefully analyzed. Although there is a large amount

of available performance data about propellers [5, 19, 23], these propellers are mostly used on commercial or military manned aircraft. On the other hand, there are no sufficiently and systematically catalogued propeller performance charts for use on small scale UAVs, except for some test results [3, 15].

As mentioned before, in ITU tailsitter UAV, the propeller system is considered to be used as main lift generating device during VTOL operations. Thus, to get the highest specific thrust (T/P) value in static and low speed climb/transition phases, a propeller with the largest plausible diameter and a relatively low pitch value should be selected. This is because, propellers with high pitch value are designed for high-speed applications and a high percentage of propeller blades are stalled during low speeds and static condition. In light of these considerations, a RASA brand 28.5×12 size (28 in. of diameter and 12 in. of pitch) propeller is selected. However, instead of wind tunnel tests, which give unsatisfactory data due to the experiment room size of ITU wind tunnel, an analytical calculation method is employed.

To derive the characteristics of the selected propeller analytically, physical modeling of the propeller's physical variables, which are pitch distribution, chord distribution and propeller's airfoil data in each section, is defined. After completing the modeling study, JavaProp software [9], which is written by Martin Hepperle, is used to analyze the propeller. JavaProp is a java based application which uses blade element theory as background theory and the validation [10] of JavaProp software has been written by Dr. Martin Hepperle with the help of comparison of the calculations using NACA's test results [22].

3.1.2 EDF Propulsion System

There are many COTS EDF units, which have 2 to 7 blades according to their size and are made from plastic or carbon fiber composite material related to the working conditions, available for the radio-control (R/C) hobby markets [8, 11]. Moreover, diameters of the commercially available EDF systems can vary between 2 and 6 in. However, like small size propellers, hobby purpose EDF units also suffer from lack of any systematically catalogued performance data. Moreover, they do not exhibit ideal ducted fan behavior because of having wider gaps between shroud and blade tips than the full size precisely manufactured ducted fans.

The general purpose and usage of the commercially available EDF systems is to mimic the full size jets on such small size R/C model aircraft, which are aimed to reach relatively high speeds such as 200 mph or more. However, such EDF systems produce less thrust than the propeller systems for a given unit power input at low speeds. This is because the blades of EDF units stall in static and low incoming velocity conditions, related to the flight-specific pitch distribution. Therefore, even though the T/P ratio of EDF systems are quite low at the static condition, second derivative of the T/P curve with respect to the airspeed is lower than the propellers' T/P curve's second derivative. Note that, there is only one unit, Schuebeler's DS51 model with available wind tunnel test measurements which is officially published on the manufacturer's website [12]. Therefore, Schuebeler DS51 EDF unit is selected for ITU Tailsitter.

3.2 Scaled Specific Thrust; A Quantitative Approach

Specific thrust, which is defined as thrust to power ratio, is the preferred method to define and compare the efficiency values of propulsion systems. Moreover, the

specific thrust value is a function of advance ratio that is also a function of angular and airspeed. So, three dimensional complex surface geometry analysis should be conducted in order to see and quantize the performance of both of the propulsion systems. However, with the help of the scaled specific thrust method, which is structured during the design phase of ITU Tailsitter UAV, the three dimensional specific thrust determination problem has scaled down to two dimensional problem. The results are plotted as seen in Fig. 3.

Moreover, the calculation method of scaled specific thrust for both EDF and propeller propulsion systems is seen in Figs. 4 and 5. Note that, for the selected "propeller based" propulsion systems, thrust and power coefficients can be written as a quadratic function of advance ratio. Therefore, the letters a_1, b_1, c_1 and a_2, b_2, c_2, which are seen in Figs. 4 and 5, are the coefficients of the quadratic equations of EDF and propeller systems respectively.

In Fig. 6, there are two regions, which are valid for our consideration. The first region is zero speed, which is simulated as hovering maneuver; the second region is from the black vertical line, which intersects the stall speed (16 m/s) on the x axis, to the desired maximum airspeed, which is 35 m per second. The pink area between "very-low" speed (0–5 m/s) and stall speed is intentionally left blank. This is because the calculation of exact and optimized transition maneuvers will be done after exact modeling of the aircraft by flight tests.

A more detailed account of the procedure is as follows; the propulsion system only overcomes parasite and induced drag from the stall speed to the maximum airspeed. However, the aircraft's weight is added to drag component, which propulsion system must overcome during the transition maneuvers. Therefore, the accurate transition phase/airspeed is investigated after calculating the optimized transition maneuvers. As seen from Fig. 6, each of the propulsion systems with any given airspeed condition results in different revolution per minute and advance ratio values. Therefore, the

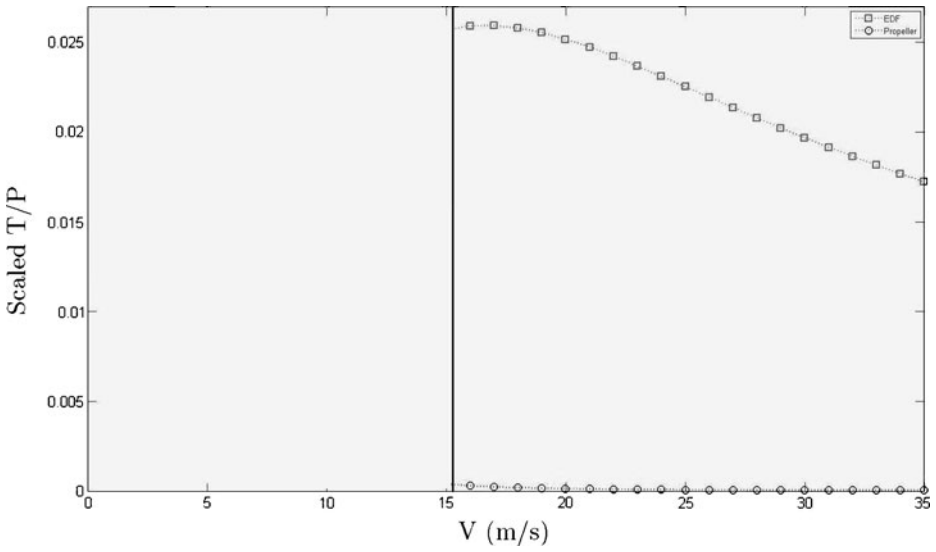

Fig. 3 Scaled specific thrust comparison of the selected propeller and EDF systems

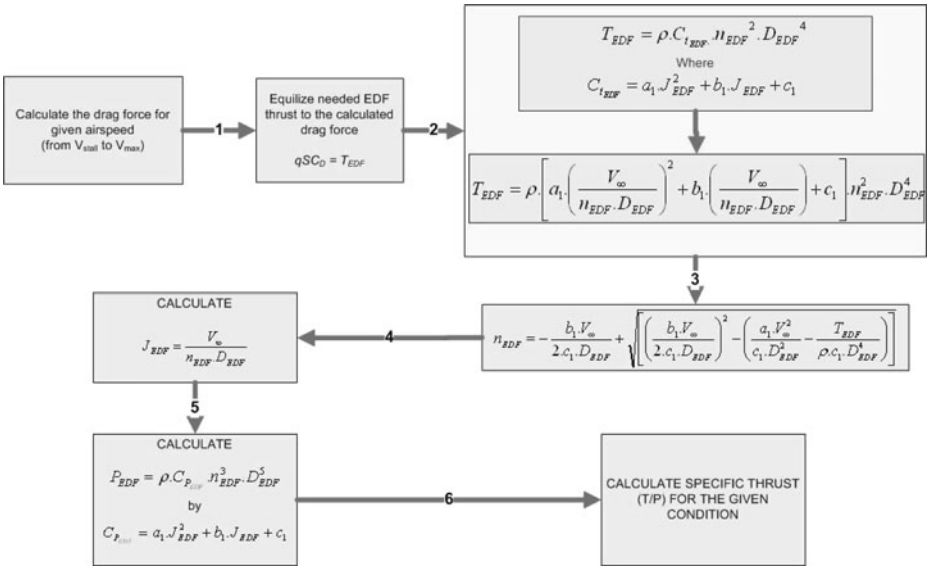

Fig. 4 Scaled specific thrust calculation methodology for EDF propulsion system

comparison between the propulsion systems can be made outright in Fig. 6. The EDF system is about 64 times more efficient than the propeller system for the whole flight regime from stall to maximum airspeed. Moreover, for static case analysis, specific thrust for both propeller and EDF systems are calculated as 0.1052 and 0.0122. Hence, depending on the static case calculations (for hover and low speed

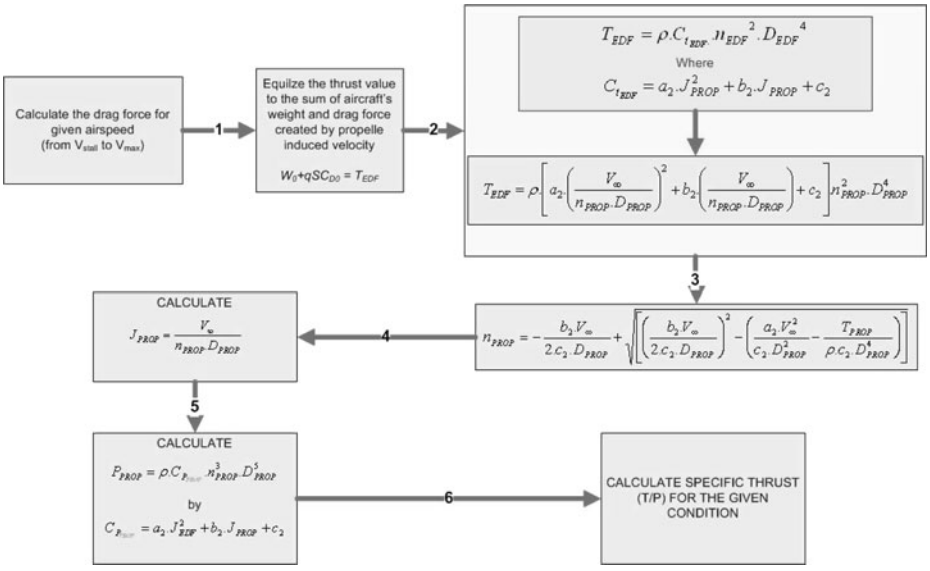

Fig. 5 Scaled specific thrust calculation methodology for propeller propulsion system

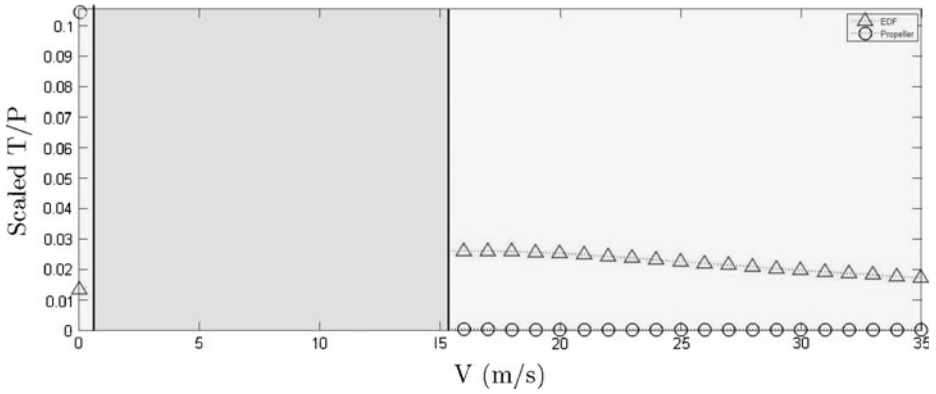

Fig. 6 Scaled specific thrust graphic for propeller and EDF propulsion systems in both hover and cruise conditions

climb) it is seen that the propeller system is about 9 times more efficient than the EDF system. However, due to angular velocity restriction, the EDF system can not produce adequate thrust as the propeller system.

As a result, the breakthrough advantage of the hybrid propulsion approach is evident in Fig. 6.

4 Optimization Based Design Methodology

The design philosophy developed hinges on obtaining the maximum possible payload capacity while achieving both high T/W ratio for VTOL, maneuverability and low energy demand per unit operation time (i.e. a low power demand for enhanced endurance). To do this, an aircraft, which has a relatively high cruise speed with vertical take off and landing capabilities, has been delineated. In addition, restrictions placed by the city operational environment were reflected via area and volume limitations before starting the design. In this section, the optimization design methodology for the ITU Tailsitter UAV is summarized.

As indicated in Fig. 7, the design methodology approach consists of three main phases. These phases are inputs, basic calculations and optimization. Input part includes two sub-parts The first sub-part is called component based constant weight inputs, which includes the weights of the components that are fixed for the design process. The second sub-part is design inputs including wing span, wing loading, maximum take off weight and the horizontal tail arm. In basic calculations part, drag coefficient, empty weight and battery weights are calculated. Optimization part is used to get most desirable design within our criteria and constraints.

4.1 Inputs

4.1.1 Component Based Constant Weight Inputs

In this part, non-variable weight inputs including electronic and power related equipments, are summarized. The components contributing to this category are

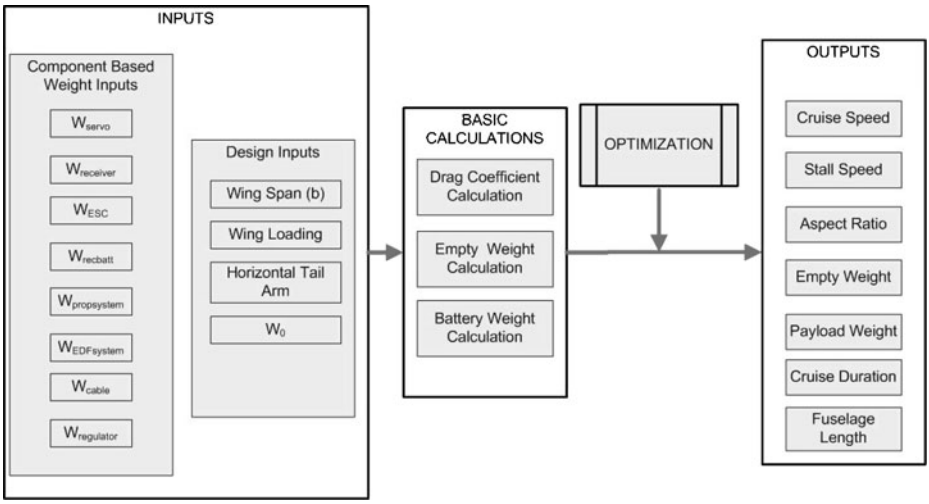

Fig. 7 General design methodology of ITU Tailsitter UAV

servos, a radio receiver, a receiver battery, electronic brushless motor drivers, a voltage regulator, cables and the brushless motors of the propulsion systems. Note that, the sum of the weight of the component based weight inputs are kept constant for each design for whole optimization process. All the components are commercial off-the-shelf (COTS) equipments and seen in Table 1.

4.1.2 Design Inputs

Design inputs consist of four variables; wing span, wing loading, horizontal tail arm and aircraft's maximum takeoff weight. Upper and lower bounds of these variables will be described and shown in optimization subsection.

4.2 Basic Calculations

4.2.1 Empty Weight Calculation

During the design process of a manned aircraft, the empty weight fraction value is generally obtained from historical data of the same size/class aircraft. Nevertheless,

Table 1 Descriptions and weights of the selected components

Component	Specifications	# of piece	Total weight (gr)
Servo	JR-DS8611 digital servo	5	215
Receiver	10 channel, PCM modulation	1	45
Receiver battery	7.4 V lithium-polymer	1	84
Electronic speed controller	Phoenix HV85 brushless ESC	2	230
Voltage regulator	7.4 volts to 6V converter circuit	1	20
Cable	Various size from 12 AWG to 24 AWG	–	57
Propeller unit	Brushless motor and propeller	–	557
EDF unit	Brushless motor and EDF unit	–	450

it's generally hard to find sufficient data to to carry out empty weight prediction for relatively novel concepts. Consequently, a quasi exact weight prediction method has been developed to calculate a "more accurate" empty weight value in terms of aircraft size and total weight for ITU Tailsitter.

Empty weight of the aircraft is composed of four main weight components as seen in Eq. 1 and these are described in detail in the following subchapters;

$$W_{empty} = W_{fuselage} + W_{wings} + W_{stabilizers} + W_{structural} \tag{1}$$

Fuselage Skin Weight Modeling Before starting the calculations, composite fabrication method had been selected. As mentioned previously, during cruise flight, the folding propeller folds onto the fuselage to reduce the drag and then the EDF system is activated. Moreover, in "cruise to hover" transition phase, EDF system is shut down and the propeller system is reactivated in order to perform a power efficient landing. It is important to note that, unfolding process of the propeller requires a symmetrical fuselage shape to prevent the propeller from damaging the fuselage skin. Therefore, in light of this prediction, a symmetrical airfoil, NACA 642-015, was selected to shape the fuselage geometry. The relation between fuselage surface area and fuselage weight was derived as a next step. The measurements on the selected fuselage airfoil show that the surface area is about 0.303 m2 for 1 meter of fuselage length. Therefore, the function for the fuselage weight can be written as given in Eq. 2 in terms of surface area and composite skin's surface weight density:

$$W_{fuselage} = 0.303 \cdot l_{fuselage} \cdot \rho_{skincomposite} \tag{2}$$

It should be noted that, l_{fuse} is the fuselage length in meters and $\rho_{skincomposite}$ is the composite skin's surface weight density in N/m2. However, fuselage length in Eq. 2 is not a sufficient parameter for the optimization problem since fuselage length depends on horizontal tail arm (l_{ht}) and root chord of the wing (C_{root}) which are variables of the optimization problem. Hence, fuselage length is expressed in terms of these variables as given in Eq. 3:

$$l_{fuselage} = l_{nose} + \frac{1}{4} C_{root} + l_{ht} \tag{3}$$

The variable l_{nose}, which is determined as a constant value of 0.4 meters, represents the distance, which is assigned by considering propeller's clearance, between the leading edge of the wing root and nose of the fuselage. Therefore, the equation of fuselage weight is derived and seen in Eq. 4.

$$W_{fuselage} = 0.303 \cdot \rho_{skincomposite} \cdot \left(0.342 + \frac{1}{4} C_{root} + l_{ht}\right) \tag{4}$$

Wing Weight Modeling During the calculation of the wing weight function; wing airfoil, taper ratio, wing loading, wingspan are the main parameters. Hence, the calculations have been started with wetted surface area of the wing. Thus, for a meter of chord length, the wetted surface area is calculated as 2.06633·b m^2, where b is the wingspan. Following these, the wing skin weight can be expressed as given in Eq. 5:

$$W_{wingskin} = 2.06613 \cdot \bar{c_{wing}} \cdot b \cdot \rho_{skincomposite} \tag{5}$$

It should be noted that, the production method and the material that is planned to be used for both the fuselage and the wing are same. Moreover, the weight of wing

spar, which is made of hollow carbon tube, must be obtained to derive the entire and accurate wing weight. Since the deflection at the tip of the wing is a crucial parameter for the wing stiffness, the tip deflection is restricted as 5 percent of the wingspan in order to be able to sustain 2.5*g* of loading. According to previous experiences, this loading condition can be modeled by applying a force equal to half the weight of the aircraft to the wing tip when the fuselage is stationary. 2.5*g* load case for the half wing can be simulated as the tip deflection of a cantilever beam loaded with a concentrated force at the free edge. The deflection is then expressed as given in Eq. 6 in detail:

$$\delta = 0.05 \cdot b = \frac{F \cdot l^3}{12 \cdot E \cdot I} = \frac{\left(\frac{W_0}{2}\right) \cdot \left(\frac{b}{2}\right)^3}{12 \cdot E \cdot I} \tag{6}$$

For the equation given above, E is the modulus of elasticity of spar material and I represents moment of inertia for a circular wing spar section. The moment of inertia can then be calculated in order to find the inner diameter of the spar, which is a hollow carbon tube. Note that, the outer diameter of the spar is restricted as given in Eq. 7:

$$\phi_{outerspar} = \left[c_{wing_{tip}} \cdot \left(\frac{t}{c} \right) \right] - 0.003 \tag{7}$$

Where $c_{wing_{tip}}$ represents the wing tip chord, $\frac{t}{c}$ represents thickness ratio of wing airfoil and the numerical value, 0.003, represents the thickness of skin composite material. Hence, the moment of inertia can be calculated as given in Eq. 8 and the inner diameter of the spar can be expressed as seen in Eq. 9. Finally, the weight of the carbon spar can be calculated in Eq. 10, given as follows:

$$I = \frac{\Pi}{4} \left[\left(\phi_{outerspar}\right)^4 - \left(\phi_{innerspar}\right)^4 \right] = \frac{\left(\frac{W_0}{2}\right) \cdot \left(\frac{b}{2}\right)^3}{12 \cdot E \cdot (b \cdot 0.05)} \tag{8}$$

$$\phi_{innerspar} = \left[\frac{4 \cdot \left(\frac{W_0}{2}\right) \left(\frac{b}{2}\right)^3}{12 \cdot \Pi \cdot E \cdot (b \cdot 0.05)} - \left(\phi_{outerspar}\right)^4 \right]^{\frac{1}{4}} \tag{9}$$

$$W_{spar} = \frac{\Pi}{4} \cdot \left[\left(\phi_{outerspar}\right)^2 - \left(\phi_{innerspar}\right)^2 \right] \cdot b \cdot \rho_{spar} \tag{10}$$

For the equation given above, ρ_{spar} is the density of the carbon material per unit volume. To conclude, after summing skin and spar weights, the weight function for the wing is derived as in Eq. 11 given below:

$$W_{spar} = \frac{\Pi}{4} \cdot \left[\left(\phi_{outerspar}\right)^2 - \left(\phi_{innerspar}\right)^2 \right] \cdot b \cdot \rho_{spar} + \left(2.06613 \cdot \bar{c}_{wing} \cdot b \cdot \rho_{composite}\right) \tag{11}$$

Stabilizer Weight Modeling The total weight of the stabilizers can be expressed as the summation of horizontal and vertical tail weights. The manufacturing method, used for the stabilizers, is slightly different from the one used for fuselage and wings. In this manufacturing technique, stabilizers are going to be made of high density foam covered with carbon fiber. Thus, wetted area and inner volume of the stabilizers are used to derive the weight function as seen in Eq. 12:

$$W_{stabilizers} = W_{HT} + W_{VT} \tag{12}$$

First of all, the calculation steps for horizontal tail are shown. After that, the calculations of vertical tail weight determination is shown.

$$W_{HT} = S_{HT_{wetted}} \cdot \rho_{skin} + v_{HT} \cdot \rho_{foam} \tag{13}$$

In Eq. 13, $S_{HT_{wetted}}$ represents the wetted area of horizontal stabilizer, ρ_{skin} represents the density of stabilizers' composite covering material, v_{HT} represents the inner volume of horizontal stabilizer and ρ_{foam} represents the density of the foam that fills the horizontal tail. Horizontal stabilizer area is written in terms of wing area, mean aerodynamic chord, tail arm and horizontal tail volume coefficient and seen in Eq. 14:

$$S_{HT} = \frac{v_{HT} \cdot \bar{c}_{wing} \cdot S_{wing}}{l_{HT}} \tag{14}$$

In the equation given above, v_{HT} is horizontal tail volume coefficient, $\bar{c}_{wing}$ is mean aerodynamic chord of the wing, S_{wing} is wing area and l_{HT} is horizontal tail arm which is equal to the distance between quarter mean aerodynamic chords of wing and horizontal stabilizer respectively. In ITU Tailsitter airplane, inverted V-tail configuration is used with 25 degree of anhedral on both left and right horizontal stabilizer parts. Therefore, the actual area of horizontal stabilizer in terms of the anhedral angle, can be calculated by using Eq. 15.

$$S_{HT_{actual}} = \frac{1}{\cos 25} \cdot \frac{v_{HT} \cdot \bar{c}_{wing} \cdot S_{wing}}{l_{HT}} \tag{15}$$

After the actual horizontal tail area is determined, wetted area can be found with respect to the tail airfoil. As indicated before, NACA0014 is selected for horizontal and vertical stabilizers. Therefore, upon inspecting the geometric properties of the selected airfoil, it is found that wetted area is 2.133 m^2 per unit planform area. Then, wetted area can easily be found as given in Eq. 16:

$$S_{HT_{wetted}} = 2.133 \cdot \frac{1}{\cos 25} \cdot \frac{v_{HT} \cdot \bar{c}_{wing} \cdot S_{wing}}{l_{HT}} \tag{16}$$

After determination of wetted area for horizontal stabilizer, the weight of the composite skin covering material can be found as given in Eq. 17:

$$W_{HT_{skin}} = 2.133 \cdot \frac{1}{\cos 25} \cdot \frac{v_{HT} \cdot \bar{c}_{wing} \cdot S_{wing}}{l_{HT}} \cdot \rho_{skin} \tag{17}$$

Next, the weight function for "foam core" must be found in order to derive weight function for horizontal tail. According to the geometrical data, the airfoil side area coefficient for one meter of chord is determined as 0.000951 fsm^2. Hence, the volume of horizontal tail is expressed as given in Eq. 18:

$$V_{HT} = \frac{v_{HT} \cdot S_{wing} \cdot c_{wing}}{l_{HT}} \cdot \left(\frac{1}{\cos 25} \right) \cdot 9.51 \cdot 10^{-4} \tag{18}$$

In order to determine the weight of foam core, the volume is multiplied by the foam density as given in Eq. 19:

$$W_{foamcore} = \frac{v_{HT} \cdot S_{wing} \cdot c_{wing}}{l_{HT}} \cdot \left(\frac{1}{\cos 25} \right) \cdot 9.51 \cdot 10^{-4} \cdot \rho_{foam} \tag{19}$$

As a result, the total weight of the horizontal stabilizer is derived by summing both foam core and skin composite weights as seen in Eq. 20:

$$\mathbf{W_{HT}} = \left[2.133 \cdot \frac{1}{\cos 25} \cdot \frac{v_{HT} \cdot \bar{c}_{wing} \cdot S_{wing}}{l_{HT}} \cdot \rho_{skin}\right] + \left[\frac{v_{HT} \cdot S_{wing} \cdot c_{wing}}{l_{HT}} \cdot \left(\frac{1}{\cos 25}\right) \cdot 9.51 \cdot 10^{-4} \cdot \rho_{foam}\right] \quad (20)$$

In similar but slightly different manner, the weight function for vertical tail is derived by using the same steps and obtained as Eq. 21:

$$\mathbf{W_{VT}} = \left[\left(\frac{v_{VT} \cdot b \cdot S_{wing}}{l_{VT}}\right) - \left(2.133 \cdot \tan 25 \cdot \frac{v_{HT} \cdot \bar{c}_{wing} \cdot S_{wing}}{l_{HT}} \cdot \rho_{skin}\right)\right] + \left[\left(\frac{v_{VT} \cdot b \cdot S_{wing}}{l_{VT}}\right) - \left(\frac{v_{HT} \cdot S_{wing} \cdot c_{wing}}{l_{HT}} \cdot \tan 25 \cdot 9.51 \cdot 10^{-4} \cdot \rho_{foam}\right)\right] \quad (21)$$

Finally, entire weight function for stabilizers is derived by summing horizontal tail and vertical tail weight functions. By inserting Eqs. 20 and 21 in the equation given below, the weight function for stabilizers is obtained as seen in Eq. 22:

$$\begin{aligned}\mathbf{W_{stabilizer}} = {} & \left[2.133 \cdot \frac{1}{\cos 25} \cdot \frac{v_{HT} \cdot \bar{c}_{wing} \cdot S_{wing}}{l_{HT}} \cdot \rho_{skin}\right] \\ & + \left[\frac{v_{HT} \cdot S_{wing} \cdot c_{wing}}{l_{HT}} \cdot \left(\frac{1}{\cos 25}\right) \cdot 9.51 \cdot 10^{-4} \cdot \rho_{foam}\right] \\ & + \left[\left(\frac{v_{VT} \cdot b \cdot S_{wing}}{l_{VT}}\right) - \left(2.133 \cdot \tan 25 \cdot \frac{v_{HT} \cdot \bar{c}_{wing} \cdot S_{wing}}{l_{HT}} \cdot \rho_{skin}\right)\right] \\ & + \left[\left(\frac{v_{VT} \cdot b \cdot S_{wing}}{l_{VT}}\right) - \left(\frac{v_{HT} \cdot S_{wing} \cdot c_{wing}}{l_{HT}} \cdot \tan 25 \cdot 9.51 \cdot 10^{-4} \cdot \rho_{foam}\right)\right] \end{aligned} \quad (22)$$

Structural Weight Modeling Structural weight consists of the weight of spar box, bulkheads, longerons and glue. Spar box weight is assumed to be a constant, while glue weight is approximated as 10% of bulkheads, longerons and spar box weights. Moreover, for building fuselage frame, it is planned to locate four longerons along the fuselage and one bulkhead per each 0.15 m of fuselage length. The total structural weight is then expressed as given in Eq. 23:

$$\mathbf{W_{structure}} = 1.1 \cdot \left(W_{bulkhead} \cdot \frac{l_{fuselage}}{0.15} + 4 \cdot l_{fuselage} \cdot W_{longeron} + W_{sparbox}\right) \quad (23)$$

Where $W_{bulkhead}$ is the assigned constant average weight of a bulkhead, $W_{longeron}$ is the weight of a carbon longeron per unit length and $W_{sparbox}$ is the preassigned constant weight value of the spar box.

4.2.2 Battery Weight Calculation

Battery Weight Modeling of The Propeller Propulsion System The propeller propulsion system is responsible for VTOL operations including hovering, low speed vertical climb and descent. To simplify the calculations, the total VTOL operation duration is set as 3 min with only hover mode. This is because, even though the

propeller consumes more energy than hovering mode during vertical climb; the energy consumption is reduced to a level below that of hovering during the vertical descent maneuver.

For hover mode, the thrust produced by the propeller is equal to the sum of weight of the aircraft and the drag force created by the propeller's induced velocity, Which is calculated using helicopter theory [2]. The battery weight determination logic for the propeller system is shown in Fig. 8 step by step.

The battery weight of the propeller propulsion system is a function of the VTOL operation duration, propeller's characteristics, drag force created by geometry of the aircraft, and the takeoff weight of the aircraft. Note that, in order to calculate the

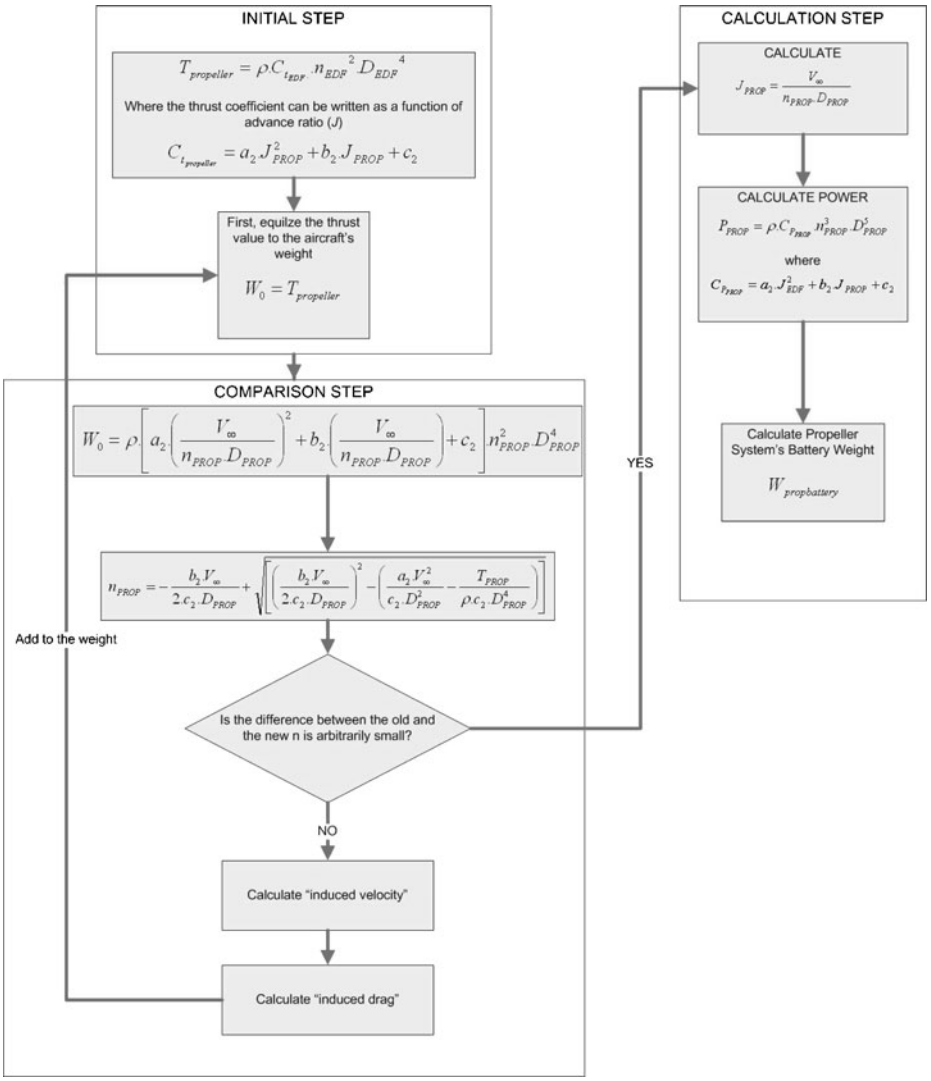

Fig. 8 Battery weight calculation steps for propeller propulsion system

"worst case" and simplify the calculations, instead of the parasite drag coefficient that is caused by the "induced velocity wetted" part of the aircraft,the parasite drag coefficient for the whole aircraft is used.

Battery Weight Modeling of The EDF Propulsion System The selected EDF unit is mainly dedicated to cruise flight. For this reason, thrust generated by the EDF unit is determined as equal to the drag force on the aircraft. Therefore, the battery weight calculation methodology is based on cruise flight and seen in Fig. 9.

4.2.3 Drag Force Modeling

The drag force of an aircraft can be written as the summation of both parasite(zero lift) and induced drags. In ITU Tailsitter design, induced drag coefficient is equalized to the parasite drag coefficient so as to fly at "minimum thrust" level. According to this drag coefficient assumption, parasite drag coefficient is the only variable that must be formulated for each design candidate during optimization process. To do that, the parasite drag coefficient of each component is calculated using the empirical

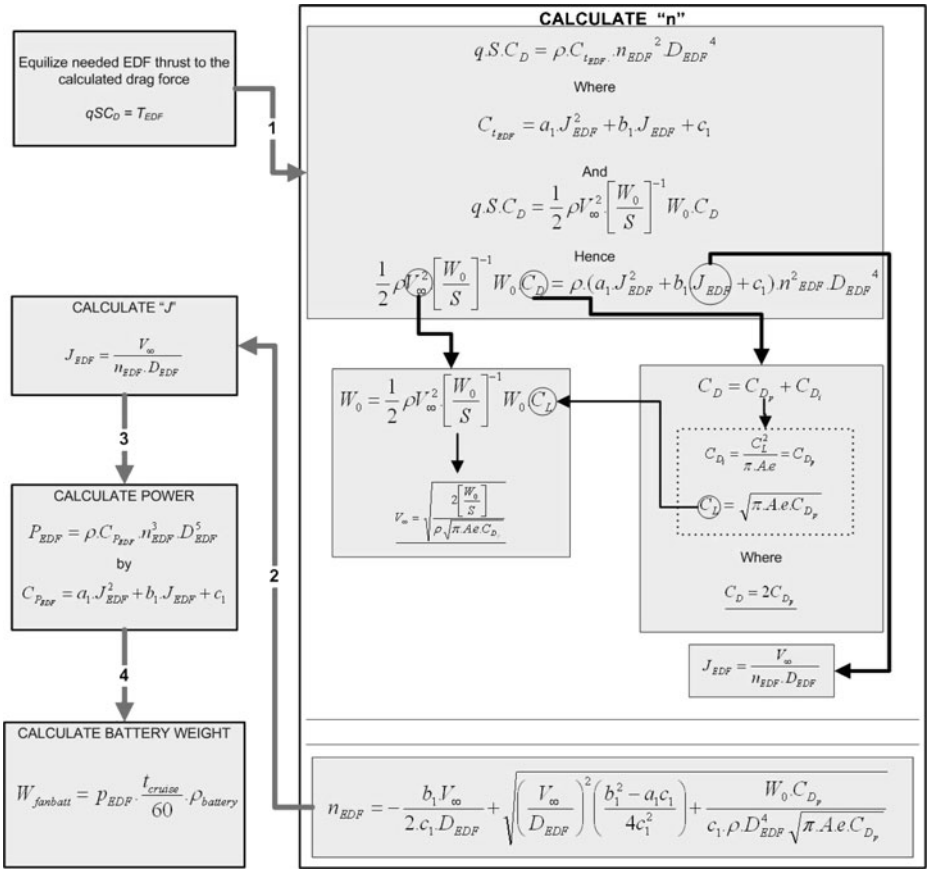

Fig. 9 Battery weight calculation for EDF propulsion unit

"component buildup" method described by Raymer [17]. According to Raymer [17] component buildup method is used to calculate drag coefficient for sub-sonic flight and counts on both flat plate skin friction and component form factor (pressure drag due to the viscous separation). Related to component buildup method, the drag coefficient of each component can be described as follow:

$$C_{D_p} = \frac{\sum C_{f_c \cdot FF_c \cdot Q_c \cdot FF_c} S_{ref}}{S_{ref}} + C_{D_{mics}} + C_{D_{LP}} \tag{24}$$

In Eq. 24, C_f denotes flat-plate skin friction coefficient, FF represents form factors, Q indicates interference factor, S_{wet} is wetted area of the selected component and S_{ref} is the reference wing area. Where the subscript "c" indicates that those values are different for each component. In the following descriptions, the equations used for each component of the aircraft are shown.

Drag Force Modeling for Aerodynamic Surfaces The parasite drag coefficient for the aerodynamic surfaces, $C_{D_{aero}}$, composed of three discrete parts; wing, horizontal stabilizer and vertical stabilizer, and figured out in Eq. 25:

$$C_{D_{aero}} = \frac{1}{S_{ref}} \cdot \left[C_{f_w \cdot FF_w \cdot Q_w \cdot FF_w} S_{wet_w} + C_{f_{HT} \cdot FF_{HT} \cdot Q_{HT} \cdot FF_c} S_{wet_{HT}} + C_{f_{VT} \cdot FF_{VT} \cdot Q_{VT} \cdot FF_{VT}} S_{wet_{VT}} \right] \tag{25}$$

Flat-plate skin friction varies depending on the type of flow, laminar or turbulent, over the surfaces. For wing and stabilizers, turbulent flow assumption has been made and flat-plate skin friction coefficient is written as Eq. 26:

$$C_f = \frac{0.455}{\left(\log_{10} Re\right)^{2.58} + \left(1 + 0.144 \cdot M^2\right)^{0.65}} \tag{26}$$

Where "Re" represents Reynolds number, which is taken 500.000 for wings and 300.000 for stabilizers; "M" indicates mach number, which is selected 0.1 as constant for each design during optimization. To continue, form factor(FF) equation for wing and tails is written in Eq. 27.

$$FF = \left[1 + \frac{0.6}{\left(\frac{x}{c}\right)_m} \cdot \left(\frac{t}{c}\right) + 100 \cdot \left(\frac{t}{c}\right)^4 \right] \cdot \left[1.34 M^{0.18} \left(\cos \Lambda_m\right)^{0.28} \right] \tag{27}$$

In Eq. 27, the term "$(\frac{x}{c})_m$" is the chordwise location of the airfoil maximum thickness point, which is 0.3 for the selected airfoils. Λ_m refers to the sweep of the maximum thickness line, which are 0 and 23 degrees for wing and stabilizers used in ITU Tailsitter respectively. The interference factor, "Q", is chosen 1.1 for both wing and stabilizers.

Drag Force Modeling for Fuselage To calculate the drag coefficient for fuselage, the steps must be followed are similar to the steps followed in wing and stabilizer calculations. However, there's a change on form factor estimation. The form factor for fuselage or smooth canopy is calculated using Eq. 28.

$$FF = \left(1 + \frac{60}{f^3} + \frac{f}{400} \right) \tag{28}$$

Where;

$$f = \frac{l}{d} = \frac{l}{\sqrt{\left(\frac{4}{\Pi}\right) A_{max}}} \tag{29}$$

4.3 Optimization

4.3.1 Defining the Optimization Problem

During the preliminary design phase, it has been observed that an aircraft which carries much more payload and flies longer would be challenging to design. Therefore, optimization process is focused on maximizing payload weight and cruise duration. Since it is not possible to optimize all the design parameters, the parameters with crucial effect are selected as primal variables of the optimization problem. Maximum Takeoff Weight (W_0), Wing Loading ($\frac{W}{S}$), Wing Span (b), Horizontal Tail Arm (l_{HT}) and Fan Battery Weight ($W_{fanbattery}$) are determined as primal variables. The boundary constraints of those variables are going to be discussed in the 'Formulation Section'. In addition, the other design constraints for the optimization problem will also form a part of the discussion in the same section. Consequently, the optimization problem can be classified as multiobjective, multidisciplinary, constrained and continuous. It is a multiobjective problem because the objective is having a maximum payload capacity with maximum cruise duration. It is a multidisciplinary optimization problem because it consists of aerodynamics, propulsion, structure and design. It is a constrained optimization since it includes both boundary and design constraints which are going to be discussed later. It is a continuous problem since the variables are free to change within the constraint space. As it was stated before, the objectives of the optimization for the ITU Tailsitter UAV can be listed as follows;

- Maximization of payload weight
- Maximization of cruise duration

Assuming the Maximum Takeoff Weight (MTOW) as a constant; the objectives, given above, are in contradiction with each other. Since maximization demand on payload weight gives the minimum cruise duration while maximization of cruise duration, which also means maximization of the battery weight, minimizes the payload weight. In light of such relations between the given objectives, the aim is to find the most suitable configuration by the optimization variables satisfying the design constraints.

4.3.2 Requirements, Variables and Constraints of the Optimization Problem

Before beginning the design process, design requirements were determined as seen in Table 2.

At the beginning of the optimization problem, MTOW, wing loading, wingspan, horizontal tail arm and fan battery weight, which are listed in Table 3, are determined to be primal variables. The constraints of the primal variables are then considered as given in Table 3 with the reasoning behind them.

In addition to the side constraints, some operational and aerodynamic restrictions are also applied to the optimization problem to obtain the desired design. At the beginning, stall and cruise speeds are assumed to be crucial parameters for

Table 2 Design requirements for the optimization problem

Minimum range	20 km
Minimum operation duration	30 min
Operation altitude	1 km
Maximum airspeed	50 m/s
Maximum operation condition wind	15 m/s
Maximum VTOL operation area	2 m × 2 m
Minimum payload weight	0.8 kg

operational capability. Stall speed is limited up to 20 m/s whereas cruise speed is limited up to 50 m/s. Moreover, in order to prevent aircraft stall due to the gust effects during cruise flight or approach, the cruise speed must be at least 5 m/s more than the stall speed. Second, although cruise duration and payload weight are being maximized via the optimization algorithm, there are lower limits which come from the design requirements.

In Table 2, it was stated that payload weight must be more than 0.8 kg, where the cruise duration must be at least 30 min. Next, in order to have an efficient, easily controllable and non-stubby design, the fuselage length is determined to be less than the wingspan. Moreover, aspect ratio's minimum value is set as 4. Consequently, all design constraints can be classified into three groups as operational capability, design requirements and geometrical limits. The determined design constraints of the optimization problem are then summarized in Table 4.

4.3.3 Mathematical Formulation of the Problem and Objective Function

In ITU Tailsitter design process, the main aim is to design an airplane which is configurable with different payload weights. To see the performance of the aircraft with different types (weight) of payloads, two objective functions have been defined; payload weight and cruise time. Therefore, in this multi-objective optimization problem, maximizing both of our objective functions is the main purpose.

Table 3 Primal variables and side constraints for the optimization problem

Primal variable	Lower bound	# upper bound	Explanation (gr)
MTOW (W_0)	30 N	100 N	Lower bound is determined according to the known weights where the upper bound is set by the structural restrictions of the propeller.
Wing loading $\left(\frac{W_0}{S}\right)$	100 $\frac{N}{m^2}$	$\frac{N}{m^2}$	The limits are based on the similar types of UAVs
b	1 m	2 m	The lower limit is set by wing efficiency issues and the upper limit is restricted by the VTOL operation area.
l_{HT}	0.6 m	1.5 m	The lower limit is determined by considering the tail size and the upper limit is set by the structural limits during vertical landing phase.
$W_{fanbattery}$	3 N	30 N	The boundaries are set by the previous experiences

Table 4 Design constraints for the optimization problem

Operation capability	$V_{stall} \leq 30\frac{m}{s}$
	$V_{cruise} \leq 50\frac{m}{s}$
	$V_{cruise} - V_{stall} \geq 5\frac{m}{s}$
Design requirements	$t_{cruise} \geq 30\ min$
	$W_{payload} \geq 8N$
Geometrical limits	$A \geq 4$
	$l_{fuselage} \leq b$

Before going into the details of objective functions, some descriptions are necessary to lay out the components of the functions. Aircraft's maximum takeoff weight (W_0) can be expressed as in Eq. 30:

$$W_0 = W_{empty} + W_{payload} + W_{fanbattery} + W_{propbattery} + W_{inputs} \tag{30}$$

Where W_{inputs} is described in Section 4.1.1 and can be reproduced here as Eq. 31:

$$W_{inputs} = W_{servo} + W_{rec} + W_{recbatt} + W_{ESC} + W_{regulator} + W_{cable} + W_{propunit} + W_{EDFunit} \tag{31}$$

In Eq. 31; $W_{servo}, W_{rec}, W_{recbatt}, W_{ESC}, W_{regulator}, W_{cable}, W_{propunit}, W_{EDFunit}$ denotes the weights of servos, receiver, electronic speed controller of the brushless motors, voltage regulator, cables, propeller propulsion unit and EDF unit respectively. In the light of the given formulations, one of the objective functions can be expressed in a compact form in Eq. 32. Note that, $W_{inputs}, W_{propbattery}, W_{fanbattery} and W_{empty}$ were described in the previous chapters as functions or invariant values.

$$FirstObjectiveFunction \longrightarrow W_{payload} = W_0 - \left[W_{empty} + W_{payload} + W_{fanbattery} + W_{propbattery} + W_{inputs}\right] \tag{32}$$

The second objective function is the cruise time for EDF propulsion system. As seen in Fig. 9, the general process to determine the battery weight for the EDF system was summarized, but not formulated. Therefore, cruise time formulation, which is seen in Eq. 33, is obtained with the help of the battery weight equation.

$$t_{cruise} = \frac{60 \cdot W_{fanbattery}}{\rho \cdot \rho_{battery} \cdot (a_2 \cdot J_{EDF}^2 + b_2 \cdot J_{EDF} + c_2) \cdot D_{EDF}^5} \cdot \frac{1}{\left[\frac{-b_1 \cdot V_\infty}{2c_1 \cdot D_{EDF}} + \sqrt{\left(\frac{V_\infty}{D_{EDF}}\right)^2 \left(\frac{b_1^2 - a_1 c_1}{4c_1^2}\right) + \frac{W_0 \cdot C_{D_p}}{c_1 \rho D_{EDF}^4 \sqrt{\pi \cdot A \cdot e \cdot C_{D_p}}}}\right]^3} \tag{33}$$

4.3.4 Optimization Methodology

After the optimization problem is discussed in detail, optimization process becomes ready to be carried through.

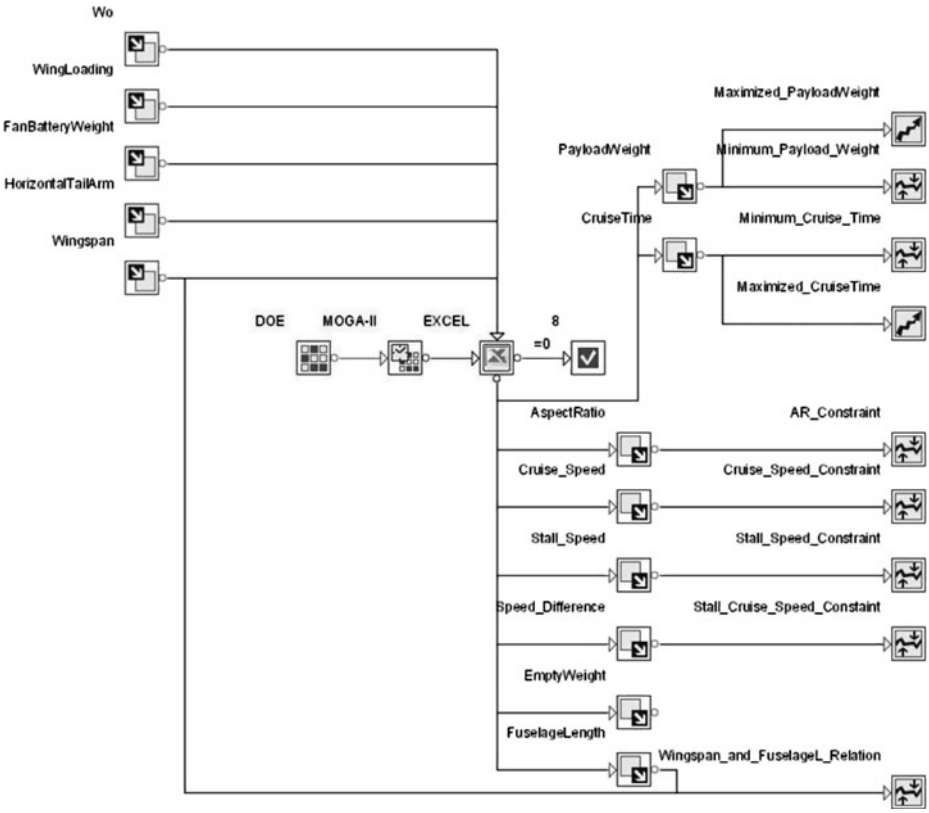

Fig. 10 Flowchart for the optimization problem

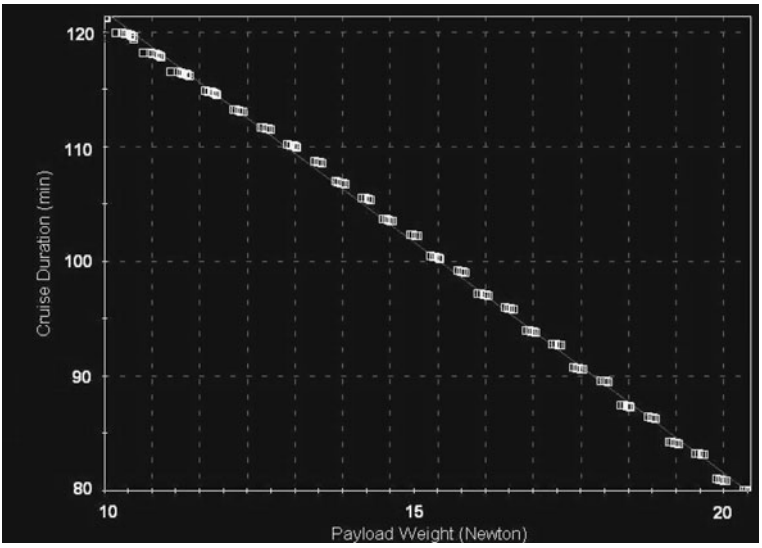

Fig. 11 Pareto graphic resulted by the optimization study

Table 5 Specifications of ITU Tailsitter UAV

Wing span	1.7	m
Wing loading	200	N/m^2
W_0	10	kg
Payload weight	∼1	kg
Cruise duration	2	hours
Range	∼90	km

Instead of developing a new code, commercially available software is preferred for the multidisciplinary design optimization of ITU Tailsitter UAV. The optimization process is decided to be performed using Esteco ModeFRONTIER 3.2 [7] as a result.

As seen in Fig. 10, the flowchart is started by adding five input nodes, which are also the previously considered optimization variables (W_0, Wing Loading, Fan Battery Weight, Horizontal Tail Arm and Wing Span). The side constraints of optimization variables are then applied to these input nodes and seven output nodes are added to the flowchart. Aspect Ratio, Cruise Speed, Stall Speed, Speed Difference and Fuselage Length output nodes are used in order to apply design constraints which are previously given in Table 4. More, Payload Weight and Cruise Time output nodes are the results of objective functions. In addition, minimum mission requirements of the optimization problem, which are given in Table 4, are also applied to these output nodes. The last output node, Empty Weight, is connected in order to monitor the empty weight of the aircraft. Multi Objective Genetic Algorithm (MOGA) is preferred for the optimization algorithm.

The results for the variables strongly depend on the optimization methodology. Thus, the methodology, which is going to be used with the optimization driver, is very important to successfully obtain an optimum design. Moreover, the Design of Experiments (DOE) node and optimization algorithm are considered carefully before starting the optimization process.

Fig. 12 3D CAD drawing of ITU Tailsitter UAV

5 Results

As stated previously, two objective functions had been determined in order to see the performance of the aircraft with different payload weights. With the help of the pareto chart, the optimization results for different configurations are seen in Fig. 11.

The final specifications and CAD drawing screenshot of ITU Tailsitter UAV are seen in Table 5 and Fig. 12, respectively.

According to the results, the tailsitter design with hybrid propulsion system has both payload and cruise duration advantages over same-class rotary wing and fixed wing alternatives. So, it shows that the accurate selection of propulsion system is one of the most vital parameters in aircraft design.

6 Conclusions

In this work, the design optimization study of a tailsitter aircraft with a revolutionary hybrid/dual propulsion system has been described. The results obtained in this paper are based on analytical calculations on the propeller propulsion system, experimental data on the EDF propulsion system and the design inputs which are in close relation with both design constraints and design criteria. Initial system performance analyses with candidate propulsion units indicate that up to 27.5 m/s cruise speed and maximum 2 hours of flight endurance, including 3 min of vertical take-off and landing duration, can be achieved while carrying a 1 kg payload and 90 km of range - a markedly superior performance in comparison to the similar class rotary-wing and OAV alternatives in the same class. As seen in Figs. 13 and 14 Prototyping of ITU Tailsitter is almost completed and flight tests are going to be conducted so as to compare real and the calculated performance.

Fig. 13 Upper fuselage and left wing photograph of ITU Tailsitter

Fig. 14 ITU Tailsitter UAV, completed view

References

1. University of Sydney: T-wing Tailsitter UAV webpage. http://www.aeromech.usyd.edu.au/uav/twing/. Accessed 20 Jan 2009 (2006)
2. Mayers, G.C., Gessow, A.: Aerodynamics of the Helicopter, 8th edn. Frederick Ungar, New York (1985)
3. Asson, K., Dunn, P.: Compact dynamometer system that can accurately determine propeller performance. J. Aircr. **29**(1), 8–9 (1992)
4. Ates, S., Bayezit, I., Inalhan, G.: Design and hardware-in-the-loop integration of a UAV microavionics system in a manned—unmanned joint airspace flight network simulator. J. Intell. Robot. Syst. **54**(1–3), 359–386 (2009)
5. Bass, R.M.: Small scale wind tunnel testing of model propellers. In: Aerospace Sciences Meeting, 24th, Reno, NV (1986)
6. Beard, R., Kingston, D., Quigley, M., Snyder, D., Christiansen, R., Johnson, W., McLain, T., Goodrich, M.: Autonomous vehicle technologies for small fixed wing UAVs. AIAA J. Aerosp. Comput. Inf. Commun. **2**(1), 92–108 (2005)
7. Esteco: Esteco modefrontier official webpage. http://www.esteco.com/ (2009)
8. Electric Ducted Fans: Ductedans.com online store. http://www.ductedfans.com/impellers_ducted_fans.html. Accessed 20 Jan 2009 (2009)
9. Hepperle, M.: Javaprop software. http://www.mh-aerotools.de/airfoils/javaprop.htm (2006)

10. Hepperle, M.: Javaprop software validation tests. http://www.mh-aerotools.de/airfoils/jp_validation.htm (2008)
11. Hobby-Lobby International Inc.: Electric ducted fans. http://www.hobby-lobby.com/ductfan.htm. Retrieved 20 Jan 2009 (2009)
12. Schuebeler Jets: Schuebeler ds51 wind tunnel test. http://www.schuebeler-jets.com/images/stories/vergleich_windkanal2.jpg. Retrieved 20 Jan 2009 (2009)
13. Knoebel, N., Osborne, S., Snyder, D., McLain, T., Beard, R., Eldredge, A.: Preliminary modeling, control, and trajectory design for miniature autonomous tailsitters. AIAA Guidance, Navigation, and Control Conference and Exhibit (2006)
14. Knoebel, N.B.: Adaptive quaternion control of a miniature tailsitter UAV. Ph.D. thesis, Brigham Young University (2007)
15. Merchant, M.P., Miller, L.S.: Propeller performance measurement for low Reynolds number UAV applications. AIAA **1127**, 2006 (2006)
16. Torres, G.E., Mueller, T.J., Srull, D.W.: Introduction to the Design of Fixed-Wing Micro Aerial Vehicles, chap. eee., pp. 39–107. AIAA (2006)
17. Raymer, D.P.: Aircraft Design: A Conceptual Approach, chap. Aerodynamics, 2nd edn., pp. 280–288. American Institute of Aeronautics and Astronautics, New York (1992)
18. Shkarayev, S., Moschetta, J.M., Bataille, B.: Aerodynamic design of micro air vehicles for vertical flight. J. Aircr. **45**(5), 1715–1724 (2008)
19. Stefko, G.L., Bober, L.J., Neumann, H.E.: New Test Techniques and Analytical Procedures for Understanding the Behavior of Advanced Propellers. NTIS, Springfield, VA (USA), 24 (1983)
20. Stinton, D.: The Design of the Aeroplane, chap. Reciprocating Engines, pp. 308–310. BSP Professional, Oxford (1993)
21. Stone, R.H.: The T-wing tail-sitter research UAV. In: International Powered Lift Conference, Williamsburg, Virginia (2002)
22. Theodorsen, T., Stickle, G.W., Brevoort, M.J., Langley Aeronautical Laboratory: Characteristics of six propellers including the high-speed range. National Advisory Committee for Aeronautics (1937)
23. Wood, D.H., NACA, Langley Research Center: Full-scale tests of metal propellers at high tip speeds. National Advisory Committee for Aeronautics, Washington, DC (1932)